J Nanopart Res (2012) 14:1072
DOI 10.1007/s11051-012-1072-5

RESEARCH PAPER

Self organization in oleic acid-coated $CoFe_2O_4$ colloids: a SAXS study

M. B. Fernández van Raap · P. Mendoza Zélis · D. F. Coral · T. E. Torres · C. Marquina · G. F. Goya · F. H. Sánchez

Received: 22 March 2012 / Accepted: 16 July 2012

Abstract We report a structural study of magnetic colloids composed of $CoFe_2O_4$ nanoparticles (mean radii in the range 2–7 nm) synthesized by thermal decomposition of different high boiling temperature organic solvents in the presence of oleic acid and oleylamine, and subsequently re-suspended in hexane. Although the surfactant layer prevents permanent aggregation and precipitation of the disperse phase, competition between attractive interactions (i.e., dipolar and van der Waals) and repulsive steric interaction leads to self organization of the magnetic nanoparticles. Our small angle X-ray scattering results evidence the presence of distinctive self organized structures in the liquid colloid depending on the type of solvent used in the synthesis. A completely homogeneous dispersion is obtained for those colloids synthesized with benzyl-ether and octadecene. Bi-disperse systems, in which nanoclusters coexist with free nanoparticles, appear when phenyl-ether and trioctylamine are used. Chain-like structures are observed in a colloid containing the particles synthesized using phenyl-ether, while more compact 3D structures form in colloids prepared with particles synthesized with trioctylamine. The presented results have important implications in the design and selection of magnetic nanoparticles for those applications where the size dispersion determines the final efficiency of the material, such as magnetic fluid hyperthermia clinical therapy.

Keywords Magnetic colloids · Aggregation · Dipolar interaction · London–van der Waals interaction · Small angle X-ray scattering

M. B. Fernández van Raap (✉) · P. Mendoza Zélis · D. F. Coral · F. H. Sánchez
IFLP-CONICET and Departamento de Física, Universidad Nacional de La Plata, Casilla de Correos 67, 1900 La Plata, Argentina
e-mail: raap@fisica.unlp.edu.ar

P. Mendoza Zélis
e-mail: pmendoza@fisica.unlp.edu.ar

T. E. Torres · C. Marquina · G. F. Goya
Departamento de Física de la Materia Condensada, Universidad de Zaragoza, Pedro Cerbuna 12, 50009 Zaragoza, Spain

T. E. Torres
Laboratorio de Microscopías Avanzadas (LMA), Instituto de Nanociencia de Aragón (INA), Universidad de Zaragoza, 50018 Zaragoza, Spain

C. Marquina
Instituto de Ciencia de Materiales de Aragón (ICMA), CSIC-Universidad de Zaragoza, 50009 Zaragoza, Spain

G. F. Goya
Instituto de Nanociencia de Aragón (INA), Universidad de Zaragoza, Mariano Esquillor s/n, 50018 Zaragoza, Spain

Introduction

An important effort is being made nowadays to improve properties of magnetic nanoparticles (MNPs) and their characterization for their use in all those

Published online: 07 August 2012

applications critically dependent on both the average particle size and particle-size distribution as in biomedical diagnostic and therapeutic applications, among others (Weinstein et al. 2010).

In some specific applications such as magnetic fluid hyperthermia (MFH) the efficiency of MNPs as heating agents when exposed to an external radio frequency (RF) field, is critically dependent on both the average particle size and size distribution (Rosensweig 2002; Gonzalez-Fernandez et al. 2009). Very recently, Bae et al. (2012) have reported extremely large values of power dissipation in nearly monodispersed magnetic cubes, confirming the key role of size dispersion on heating properties. Although great effort is dedicated to MNP improvement, structuring analysis in the colloid is barely performed. The enhancement of colloidal properties requires a systematic analysis of the aggregation within the liquid carrier that is known to occur (Benkoski et al. 2007). Aggregations may lead to thermal conductivity increase (Evans et al. 2008) due to the ability of the heat to move rapidly along the backbone of the cluster. This increase may result in heat sinking that for example in the case of using MNPs for MF, would lead to lowering tissue heating effectiveness and damaging healthy nearby tissue. Also large thermal conductivity enhancement is accompanied by sharp viscosity increase at low nanoparticle volume fractions (<1 %) (Kwak and Kim 2005; Zubarev et al. 2002). The net magnetic moment and magnetic anisotropy of the MNPs composing a magnetic colloid are also expected to influence the degree of magnetic interaction among particles, and therefore the formation of oligomeric structures like dimers, chains, rings, etc. This in turn could affect macroscopic properties of the colloid such as the already mentioned and consequently the heating properties during MFH treatments. A complete discussion on the role of the magnetic anisotropy on the specific absorption rate of cobalt-ferrite nanoparticles has been addressed by Verde et al. (2012). Co-induced enhancement of these two parameters and is expected to increase dipolar interactions and, in consequence, the aggregation tendency.

Co-ferrite is often synthesized by coprecipitation. This type of synthesis produces a relatively large amount of material, but size and polydispersity control is difficult. In the contrary, thermal decomposition of metal-oleate precursors in a high boiling temperature solvent produces hydrophobic nearly monodisperse nanocrystals (Kim et al. 2011; Park et al. 2004).

Small angle X-ray scattering (SAXS) is an appropriated technique to investigate morphology and structure of colloids at various length scales simultaneously. A main difference with other characterization techniques relies on the fact that by the SAXS technique MNP are observed in the real fluid state. Aggregation and self organization with a tendency to chain-like structure formation due to dipole–dipole interaction have been observed under an applied magnetic field in polydisperse (core radius $r \sim 5$ nm and standard deviation $\sigma \sim 2$nm) magnetite-coated with oleic acid (OA) in Isopar-m oil (Kruse et al. 2003a, b), and without field in charge-stabilized colloids of uncoated iron oxyhydroxide (FeOOH) in water (Gilbert et al. 2007), in Co ferrite ($r \sim 4$ nm and $\sigma \sim 0.15$ nm)-coated with OA in cyclohexane (Bonini et al. 2007), and in alkanoic acid stabilized magnetite ($r \sim 5$ nm and $\sigma \sim 1.5$ nm) in aqueous and organic solvents (Shen et al. 2001).

Here, we apply the SAXS technique, using synchrotron radiation, to analyze colloids of $CoFe_2O_4$ MNP-coated by OA (OA–$CoFe_2O_4$) and resuspended in hexane. These MNPs were specially designed for MFH applications (Torres et al. 2010), in the sense that solvent was systematically changed to vary primary particle mean size and very low primary particle polydispersity is achieved. These results contribute to a better understanding of the interplay between isotropic and anisotropic interactions favoring the formation of 3D or linear structures.

Materials and methods

Colloids synthesis and characterization

$CoFe_2O_4$ nanoparticles of different sizes were prepared by thermal decomposition of iron (Sun et al. 2004; Roca et al. 2006), acetylacetonate $Fe(acac)_3$ and cobalt acetylacetonate $Co(acac)_2$ as organic precursors. The adequate proportions of $Fe(acac)_3$, $Co(acac)_2$, OA, oleylamine and the corresponding solvent were mixed and stirred under N_2 flow. Summarizing, for a typical preparation, 10.4 mmol of $Fe(acac)_3$ and 5.2 mmol of $Co(acac)_2$ were dissolved in 52 mmol of OA, 65.4 mmol of Oleylamine, 86.5 mmol of 1,2-octanediol, and 150 ml of solvent. The mixture was

heated to 200 °C and held at this temperature for 2 h to promote nucleation. After that it was heated in a N_2 environment to the boiling temperature, to reflux for another time interval t_r (Torres et al. 2010) to allow particle growth. Different solvents were used: phenyl ether, benzyl ether, 1-octadecene, and trioctylamine, having boiling temperatures of 538, 573, 593, and 638 K, respectively, in order to control the final particle size. The labels for the colloids synthesized using different solvents are indicated within brackets: benzyl ether (C_{be}), phenyl ether (C_{pe}), 1-octadecene (C_{od}), and trioctylamine (C_{tA} and C_{tB}). Precursor to surfactant molar ratio was 1:3, and t_r was 60 min for C_{pe} and 30 min for the other colloids.

Transmission electron microscopy (TEM) images were obtained with a thermoionic 200 kV Tecnai T20 microscope on samples prepared by dropping the colloids onto a TEM grid and subsequent evaporation of the solvent. Details on preparation of OA–$CoFe_2O_4$ MNP and magnetic colloids, on their magnetic properties and on other structural characterization will be discussed in other study.

Small angle X-ray scattering experiments

SAXS experiment was performed at D11A-SAXS beamline (Kellermann et al. 1997) at the Laboratorio Nacional de Luz Sincrotron (LNLS) in Campinas, Brazil. All data were collected at 300 K using 300k Pilatus bidimensional detector at a wavelength, $\lambda = 1.488$ Å. Interacting systems often derived in structures displaying hierarchical assemblies demand the observation in a wide scattering vector (q) range. A q range from about 0.06 to 6 nm^{-1} was covered using two sample-detector distances of 659 and 1360 mm. Maximum resolution in scattering vector ($\Delta q = 0.01$ nm^{-1}) is achieved for the longer camera length and detector pixel size (172 μm). Camera length was calibrated using the lamellar structure of silver behenate (Huang et al. 1993). The scattering intensity was measured as function of $q = 4\pi \sin(\theta)/\lambda$, where 2θ is the scattering angle. For the measurement the samples were injected in between two clear Ruby Mica Discs, 25 μm thick each, of the liquid sample holder. Correction for background scattering and from hexane density fluctuation was done by subtracting to the data, previously corrected by absorption, the scattering registered from sample holder filled with hexane. After that, absolute calibration of the measured (arbitrary) intensity $I(q)$ to the differential scattering cross section per unit volume of irradiated sample, $\frac{\partial \Sigma}{\partial \Omega}$, in units of cm^{-1}, was achieved using water as a secondary standard, following the procedure described elsewhere (Orthaber et al. 2000). The correctness of the procedure was verified noticing that data acquired with the two used camera lengths naturally matches after calibration. SAXS was registered from the as-synthesized MNP re-suspended in hexane to the concentrations listed in Table 1, determined by atomic emission spectroscopy–inductively coupled plasma (AES–ICP). SAXS represents a statistical average of the scattering measured from the irradiated volume with a typical spot size on the sample of 2 (h) × 1 (v) mm^2.

Results

A representative TEM image of the OA–$CoFe_2O_4$ nanoparticles studied here is shown in Fig. 1a for the

Table 1 SAXS and TEM results

Colloid label	C (g l^{-1})	ϕ (10^{-3})	r_m (nm)	σ_s (nm)	r_T (nm)	σ_T (nm)	d_f	$\Delta\eta$ (10^{-3} nm^{-2})	α
C_{be}	27.8	6	4.177	0.558	4.40	0.625	–	2.90	0
C_{od}	5.0	1	6.635	0.601	6.63	0.558	–	3.13	0
C_{pe}	16.6	3	1.886	0.387	2.50	0.375	1.33	3.55	0.34
C_{tA}	10.8	2	5.446	0.802	5.40	0.726	2.99	1.22	0.38
C_{tB}	13.7	3	5.649	0.951	6.56	1.401	2.89	1.47	0.20

C stands for concentration as OA–$CoFe_2O_4$ mass per colloid volume; ϕ, for volume fraction obtained using $CoFe_2O_4$ density equal to 4,600 kg m^{-3}; r_m, for the median value of particle radii resulted from SAXS data analysis with a lognorm standard deviation $\sigma_s = r_m e^{\sigma^2/2}\sqrt{e^{\sigma^2}-1}$, being σ the standard deviation of the Gaussian distribution of $\ln r/r_m$; d_f, for the fractal dimension of the aggregates; $\Delta\eta$, for the scattering length difference between MNP core and hexane; α, for the fraction of aggregated nanoparticles; r_T and σ_T, for the mean radii and standard deviations from Gaussian fits of TEM histograms

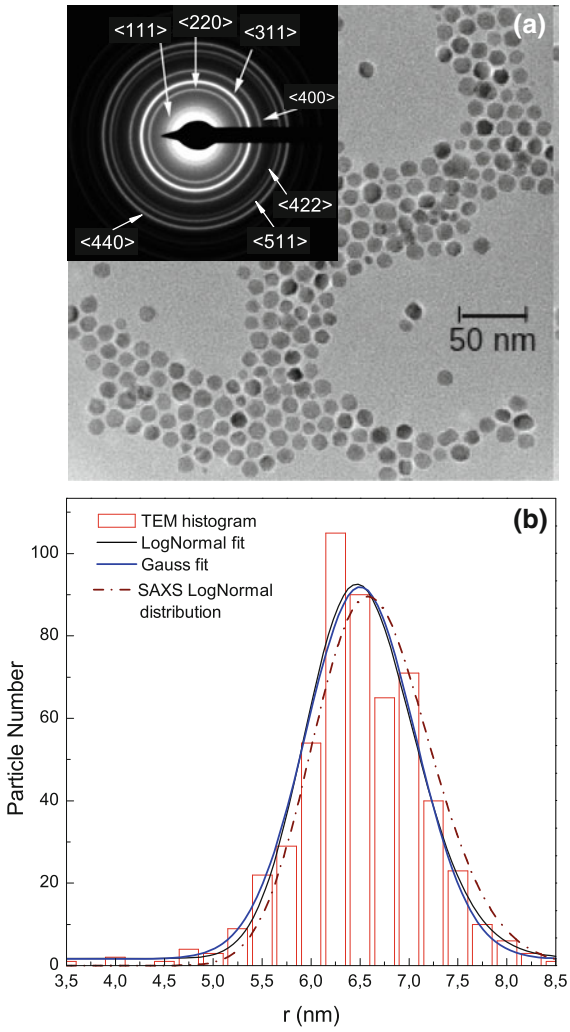

Fig. 1 **a** TEM image of C_{od} colloid, *inset* (**a**) selected area electron diffraction pattern. **b** Radii histogram from TEM micrograph with its Gaussian and log norm fits. The log normal distribution derived from SAXS analysis is superimposed to TEM histogram showing the agreement between SAXS and TEM results

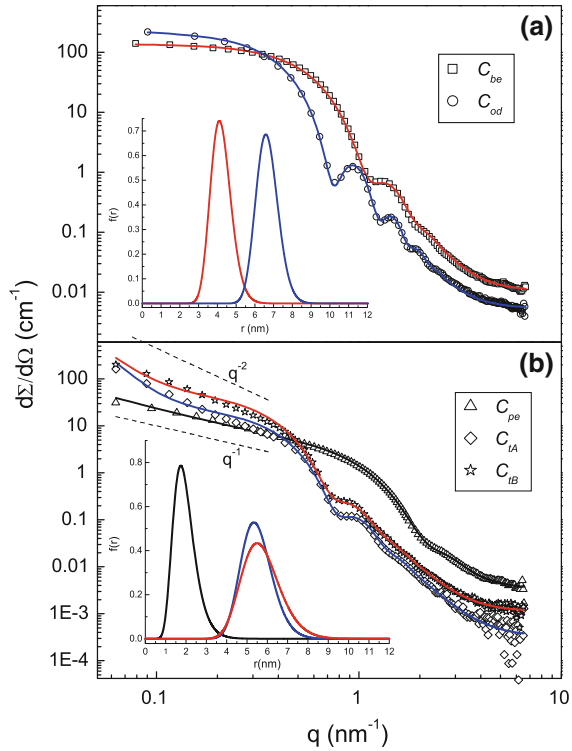

Fig. 2 Double-logarithmic representation of scattering curves from non-aggregated magnetic colloids (**a**), where full lines stand for best fit results and the *inset* shows the resulting radii distributions derived from best fits with Eq. 2 holding $S(q)$ fixed equal to 1 and $\Delta\eta_2 = 0$; and from aggregated magnetic colloids (**b**), where full lines stand for best fit results with Eq. 4 keeping $\Delta\eta_2 = 0$. The *insets* show the resulting radii distribution

C_{od} sample. The particles are nearly spherical and monodisperse. Selected area electron diffraction pattern shown at the inset of Fig. 1a indicates good nanoparticle crystallinity and was indexed with a cubic spinel structure (space group *Fd3m*). Some clustering is observed; this kind of arrangement is influenced by the wettability of the TEM-grid surface during the sample deposition and drying. An estimation of the OA coating thickness can be inferred from the minimum particle separation in the TEM micrographs. The size distribution obtained by measuring more than 500 particles and the best fit with a Gaussian distribution are shown in Fig. 1b. The fitted parameters, mean radius (r_T) and standard deviation (σ_T) are listed in Table 1. From the analysis of TEM images, it can be inferred that the MNP produced by thermal decomposition are nearly uniform in size, with mean radii in the range 2–7 nm and coating thickness size around 2 nm.

Figure 2 shows a double logarithm representation of scattering curves of the magnetic colloids. Not all these patterns have the same overall curve shape and therefore were plotted in two separated graphs. Scattering curves of C_{be} and C_{od} samples are displayed in Fig. 2a. These SAXS patterns are associated to complete colloidal dispersions; the curves correspond to typical particulate systems, showing at low q region a behavior close to a Guinier law, indicating very low polydispersity and no aggregation. In the central part of the curves, fringes are clear but somehow smooth due to the finite-size

distribution. At large q range a Porod type law q^{-4} characteristic of smooth individual particle surfaces appears. The SAXS curves of C_{pe}, C_{tA}, and C_{tB} samples, shown in Fig. 2b, differ from the previous ones at low q range, where a power law behavior is observed instead of a Guinier type behavior, indicating that MNP aggregation has occurred. At the high q region the scattering is dominated by the particle structure factor with the Porod type behavior.

To take into account the MNP aggregation, scattering curves analysis was performed using the analytic form of the structure function $S(q)$ derived for a fractal model of aggregation, in which the power law form of the scattering function is limited by finite cluster size ξ and by the primary particle finite size (radius r_0), appearing in the pair correlation function as an exponential cut-off $h(r, \xi) = \exp[-r/\xi]$ and a $\delta(r)$, respectively (Freltoft et al. 1986; Chen and Teixeira 1986). The structure factor $S(q)$ is given by:

$$S(q) = 1 + \frac{d_f \Gamma(d_f - 1)}{(qr_0)^{d_f}} \frac{\sin((d_f - 1)\tan^{-1}(q\xi))}{(1 + 1/(q\xi)^2)^{\frac{d_f - 1}{2}}}, \quad (1)$$

where, Γ is the gamma function and d_f the fractal dimension. The aggregate fractal dimension arises from the scaling relationship between mass (or particle number) and enclosed volume, and is a measure of how the particles are packed and provides insight into clustering shape.

The differential cross section curve is given by:

$$\frac{\partial \Sigma}{\partial \Omega} = N_p P(q) S(q) + \text{bkg}, \quad (2)$$

where "bkg" is the incoherent background and N_p is the particle number density. $P(q)$ is the core-shell form factor function for polydisperse spherically symmetric particles with mean radius size r_0 and shell thickness t_c,

$$P(q) = \int_0^\infty f(r)(K(q, r + t_c, \Delta\eta_2) - K(q, r, \Delta\eta_2 - \Delta\eta_1))^2 dr, \quad (3)$$

being $f(r)$ the radii distribution and $K(q, r, \Delta\eta) = 3\Delta\eta V_p \frac{\sin(qr) - qr\cos(qr)}{(qr)^3}$ for a spherical particle of radius r and scattering length density differences between particle and matrix $\Delta\eta$. $\Delta\eta_1$ and $\Delta\eta_2$ are the scattering length density difference between MNP core and hexane, and between OA shell and hexane, respectively. Equation (3) turns to core form factor for $\Delta\eta_2 = 0$. The scattering length densities of $CoFe_2O_4$, OA and hexane are 3.942×10^{-3}, 0.807×10^{-3}, and 0.646×10^{-3} nm^{-2}, respectively. Therefore, the contrast between OA and hexane is only 5 % of Co-ferrite/OA contrast, situation that makes the coating layer almost undetectable by both SAXS and TEM.

Although radius particle distributions obtained from TEM histograms very closely matche a Gaussian profile and good fits can be obtained with both Gaussian and lognormal distributions (see Fig. 1b), for SAXS analysis the log-norm distribution function $f(r)$ was chosen to avoid ad-hoc symmetry impositions as it is suggested in previous work for quasi-spherical, highly monodisperse and crystalline nanoparticles (Borchert et al. 2005).

Scattering curves of magnetic colloids without interparticle correlations like those in Fig. 2a, were nicely fitted with Eq. 2 using a structure function equal to 1. Fit goodnesses obtained using core-shell form factor or only core factor (Eq. 3 with $\Delta\eta_2 = 0$) are quite similar, and there is almost no change in fitted parameters related to core particle electronic density, size, and dispersion. For instance, simulations of a colloid scattering curve of 6 nm Co-ferrite core radius with 2 nm OA shell and without shell display minor differences, like a shift in fringe positions smaller than q resolution, and indistinctive intensity variations.

In the case of magnetic colloids displaying aggregation like those in Fig. 2b, it was not possible to fit simultaneously the data in the whole q range with Eq. 2. For this reason it was modified in the following way

$$\frac{\partial \Sigma}{\partial \Omega}(q) = N_p P(q)(1 - \alpha + \alpha S(q)) + \text{bkg}, \quad (4)$$

straightforwardly assuming a fraction of particles $(1 - \alpha)$ which do not form part of an aggregate, coexisting with a fraction α of aggregated particles. It can be seen in Fig. 2b, that Eq. 4 with core form factor is good enough to fit the data in the whole q range. In the range $q\xi \ll 1$ the data should show a trend toward saturation due to finite aggregate size. This behavior is not observed because the crossover related to ξ is out of our data range. A $S(q)$ analysis indicates that this function is more sensitive to changes in r_0 and d_f than to those in ξ. Then fits were carried out with ξ fixed at 100 nm, which is the smallest possible value

compatible with our first data point through $2\pi/\xi = 0.06$ nm^{-1}. Fitted parameters, listed in Table 1 together with TEM derived ones, were: the median core radius r_m, the core size polydispersity σ_s, the fractal dimension d_f, the scattering length density difference between MNP and hexane $\Delta\eta$ and the fraction of aggregated particles α. The accord between SAXS primary particle values and TEM structural parameters (size and standard deviation) is excellent. Figure 1b shows the MNP radii distribution derived from the SAXS pattern superimposed to TEM histogram. Theoretical length density difference between $CoFe_2O_4$ ($\rho = 4{,}900$ g cm^{-3}) and hexane is 3.296×10^{-2} nm^{-2}. The fitted $\Delta\eta$ values are in good agreement with $CoFe_2O_4$, although for C_{tA} and C_{tB} is considerably low. From fitted fractal dimension d_f values it can be inferred that nanoparticle self organization occurs in a chain like connected network structure in the C_{pe} colloid, while a more dense and compact 3D structure forms in C_{tA} and C_{tB}.

Discussion

Our SAXS results on OA–$CoFe_2O_4$ nanoparticles prepared using various high boiling temperature solvents and resuspended in hexane, evidence different structures: a completely homogeneous dispersion is obtained for those colloids synthesized with benzyl ether and octadecene, and clustering as a bidisperse system in which nanoclusters coexist with free nanoparticles is observed for the other solvents. The description in terms of this coexistence may reflect the occurrence of thermal equilibrium between aggregated and no aggregated MNP states having comparable energies. The presence of chain base like structures is observed for the colloid synthesized using phenyl ether, while more compact 3D structures are formed in colloids synthesized with trioctylamine. No correlation between concentration C and structural data can be inferred from data in Table 1 for the narrow concentration range, corresponding to volume fraction $\phi = C\,\rho^{-1}$ between 1×10^{-3} and 6×10^{-3}, also listed together with structural data.

Self organization and aggregation between MNP is usually analyzed as the result of a competition between anisotropic attractive dipole–dipole interaction energy (E_{dd}) which favors the formation of 1D chain like structures, isotropic London–van der Waals attraction energy (E_{vdW}) which favors 3D spherical like structures, and steric repulsion energy (E_s). The steric repulsion was taking into account not allowing interpenetration between OA molecules of adjacent particles. The coating is assumed as a rigid layer of thickness t_c and E_s equal to ∞ for separation between cores surfaces $d_c \leq 2\ t_c$ and zero for $d_c > 2\ t_c$. No electrostatic interaction was introduced, since the charge can only arise from dissociated carboxyl groups which are bound to MNP surface.

The appearance of self organization is analyzed in terms of the ratio of total interaction energy E_T between two particles and their thermal energy equal to $2k_BT$ through the aggregation parameter λ_A (Kruse et al. 2003b; Rosensweig 1997). This parameter is defined as $\lambda_A = \frac{|E_{vdW}+E_{dd}|}{2k_BT}$. Aggregates may exist when $\lambda_A > 1$. E_{vdW} values were computed with the formula derived by Hamaker (1937) for two spherical equal particles interacting across a medium.

Hamaker constant $A_H = \left(A_{H_{MNP}}^{1/2} - A_m^{1/2}\right)^2$ depends on the dielectric properties of the involved materials (MNP) and the intervening medium (m) and determines the strength of van der Waals interactions. For Fe and their oxides in hydrocarbon A_H lies in the range from 0.3×10^{-19} to 3×10^{-19} J (Hamaker 1937). A_H for the surfactant shell (Kruglyakov 2000) is 2.45×10^{-20} J and for the solvent medium (Croucher and Hair 1977) (hexane) is in the range from 3.8×10^{-20} to 5.48×10^{-20} J. These two values are close and one order of magnitude lower than the $CoFe_2O_4$ Hamaker constant ($A_{H_{MNP}}$). A_H of $CoFe_2O_4$ is not precisely known and recently calculated values in nonpolar solvents are much lower than previous experimental reports (Faure et al. 2011). Here $A_H = 2.7 \times 10^{-19}$ J is used.

E_{dd} depends on the magnitude of the distance vector between the centers of the two dipoles and on the angles φ_1, φ_2 between this vector and the magnetic moment directions. Values listed in Table 1 correspond to the configuration that minimizes the energy at $\varphi = \varphi_1 = \varphi_2$ (nose-tail configuration), and were calculated considering that the core of small particles consists of a magnetic nucleus r_{mag} plus a magnetic dead shell due to spin canting at the surface (Coey 1971). Table 2, E_{dd}, E_{vdW}, and λ_A values calculated for some of our colloids are listed. The magnetic radii r_{mag} values were estimated from the comparison of

Table 2 Calculated values of M_s, r_{mag}, t_c, E_{dd}, E_{vdW}, λ_A, ζ, and V_m

Colloid label	M_s (A m^2 kg^{-1})	r_{mag} (nm)	t_c (nm)	E_{dd} (10^{-3}eV)	E_{vdW} (10^{-3}eV)	λ_A	ζ	V_m (nm^3)
C_{be}	40.2	1.94	1.20[a]	−0.2	−39	0.75	438	0.33
C_{od}	67.3	3.88	1.75	−2.9	−47	0.96	1106	0.46
C_{pe}	17.1	0.73	1.50	−0.002	−90	1.30	90	0.81
C_{tA}	48.1	2.61	1.0	−0.6	−99	1.93	745	0.23

M_s, is the experimental saturation magnetization obtained at $\mu_0 H = 320$ kA m^{-1} and 400 K; r_{mag}, stands for magnetic mean radii inferred from M_s; t_c, for coating mean thickness inferred from TEM; E_{dd}, for dipole-dipole energy of the nose-tail configuration; E_{vdW}, for van der Waals energy calculated using Hamaker approximation with $A_H = 2.7 \times 10^{-19}$J; λ_A, for the aggregation parameter at $2k_BT = 5.17 \times 10^{-2}$ eV ($T = 300$ K); ζ, for the amount of OA molecules attached to the NMP surface and V_m for the volume available per molecule. C_{tB} data is not listed because this colloid is similar to C_{tA} under experimental uncertainties

[a] t_c for C_{be} was not measured but, calculations covering a range from 1 to 1.75 nm result in a λ_A value smaller than 1

measured saturation magnetization values M_s (with $CoFe_2O_4$ bulk value of 92.3 A m^2 Kg^{-1}) and coating thickness t_c derived from TEM. These t_c values are within the expected range taking into consideration that the size of one OA molecule ($C_{18}H_{34}O_2$) can be estimated as 1.97 nm length and 0.5 nm width, and that OA molecule gets chemisorbed as a carboxylate on the metallic atoms of the nanoparticle surface (Wu et al. 2004).

The calculated λ_A value for C_{be} and C_{od} are smaller than 1, indicating that if two particles aggregates forms, the bond can break due to thermal energy, in accord with SAXS data, that display no aggregation. For C_{tA} and C_{tB} which are quite similar samples, λ_A value is close to 2, also in agreement with SAXS pattern that displays aggregation. Similar results have been predicted from Monte Carlo simulation of a 3D pure dipolar hard-sphere system of volume fractions $\phi \sim 10^{-3}$, i.e., cluster formation of quasi spherical shapes with fractal dimensions close to 3 and the appearance of a bidisperse system in which nanoclusters coexist with free nanoparticles (Pshenichnikov and Mekhonoshin 2001). It can be noticed that $|E_{dd}| \ll |E_{vdW}|$ for all the colloids studied here, so the behavior is strongly influenced by E_{vdW}.

MNP in the C_{pe} colloid are very small, mean radius smaller than 2 nm, and display a more open self organized structure with a d_f value of 1.33. For this sample the assumption of a rigid OA coating may not be valid. An estimation of the number ζ of OA molecules attached to the MNP surface, is achieved assuming that each adsorbed molecule covers an area of $A_m = 0.5$ nm^2. ζ value for C_{pe} is quite small comparing with the other colloids (see Table 2). The tail of the OA molecule can take any orientation due to thermal motion, within a cone centered at its attachment position on the MNP surface and limited by a base area equal to $4\pi(r + t_c)^2/\zeta$. The volume per OA, where the molecule can take any orientation, is $V_m = (1 + t_c/r)^2 t_c\, A_m/3$. Calculated values of ζ and V_m are listed in Table 2. The shorter r the larger V_m. Therefore, for C_{pe} V_m is at least twice larger than the other colloids studied here, large enough to confidently suggest that the assumption of a rigid coating layer does not hold (see Table 2). When the distance between particle surfaces becomes less than t_c, the molecules attached to particle surface compress each other resulting in an elastic repulsion and a loss of configurational entropy. A case where this kind of steric interaction compensates the strong isotropic van der Waals may lead to anisotropic interaction E_{dd} to prevail and to chain formation, particularly at $\varphi = \pi$ where the dipolar force is stronger. For this case, our calculations predict that MNP smaller than 2.6 nm can avoid agglomeration, therefore this model still does not explain the C_{pe} result completely. A larger number of attached OA molecules per MNP for samples displaying larger M_s is in agreement with recent research, reporting that oleic, dodecanoic, and citric acids act in order to decrease the spin disorder at the surface of the MNP, enhancing M_s values (Barbeta et al. 2010). OA adsorption efficiency may depend on the solvent used and other synthesis parameters, therefore inducing additional differences in the self organization behavior of samples studied here.

Fractal exponent d_f values in the range 1.06–1.26 have been related to dipolar long range interaction assuming energy minimization achieved by moment alignment in a nose to tail manner (Bonini et al. 2007; Kruse et al. 2003b); also values in the range 1.1–1.2

have been reported for charge stabilized colloids (Gilbert et al. 2007) where a repulsive electrostatic energy barrier has to be overcome for further aggregation. In those cases as here, SAXS data analysis was carried out using the structure factor given by Eq. 1, which was derived in a purely geometric way, without taking into consideration long-range interactions. To our knowledge, there is no theoretical accepted model that takes into account long-range interactions in the structure function.

We stress the fact that the MNP characterization in the fluid state is extremely important since it allows to study, quantify, and predict the appearance of clustering, that can restrict the practical applications of the MNP, as well as to retrieve insight on its morphology and polydispersity. The colloid structural properties determine thermal conductivity enhancement (Kwak and Kim 2005), related magnetoviscous effects, and the response of the suspended MNP to static and dynamic magnetic fields. These properties affect the efficiency of MNP transport using magnetic field gradients, the power absorption under RF irradiation, and the subsequent power dissipation. Results reported here, are valuable for future similar study to be pursued in aqueous colloids, after MNP surface hydrophobicity modification by bipolar surfactant addition, because medium replacement from hexane to water, may lead to same order of magnitude of E_{vdW} as the A_H constant for water (3.7×10^{-20} J) is close to the hexane one.

The present analysis in terms of an aggregation parameter supports previous studies that indicate that van der Waals interaction yields a significant contribution and cannot be neglected (Kruse et al. 2003a). Furthermore, our work showed that the steric interaction, determined by coating molecules arranging and their entropy and mobility, is also relevant. The resulted NMP arrangement may be used as input for computational evaluation of the role of dipole–dipole interactions at RF heating of MNPs ensembles (Haase and Nowak 2012). Heating power dependence versus concentration as obtained in this reference can drastically change using the colloidal structure here obtained.

Conclusions

The structure of colloids containing nearly monodispersed OA-coated $CoFe_2O_4$ MNP, synthesized by thermal decomposition and resuspended in hexane, was probed in the absence of a magnetic field at room temperature with SAXS technique using synchrotron radiation. Our experimental results display that depending on the high boiling point solvent used during the synthesis procedure, completely homogeneous dispersion or inhomogeneous bi-dispersed systems appear. For the latter, interconnected chain like structure and more dense and compact clusters were found.

Self organization analyzed in terms of the interplay between isotropic steric repulsive effects due to surfactant layer (modeled as a rigid layer), isotropic attractive van der Waals and anisotropic attractive dipolar interactions can be understood for colloids composed of particles with mean radius larger than 4 nm. A colloid containing smaller particles ($r < 2$ nm) displays an interconnected chain like structure that may be understood in terms of these interactions but with the assumption that coating molecules leave more available volume and have larger mobility allowing OA molecules interpenetration. Although the aggregation mechanism is still not completely understood, the topological characterization of the colloids carried out here is of crucial importance for further improvements in nanoparticle design for biomedical applications like MFH.

Acknowledgments We thank financial support from: LNLS synchrotron, Campinas, SP, Brazil under proposals D11A-SAXS1-9293, CONICET (PIP 01111) and ANPCyT (PICT 00898) of Argentina and the Spanish Ministerio de Ciencia e Innovación (projects MAT2010-19326 and CONSOLIDER NANOBIOMED CS-27 2006). Valuable help of Dr. A. Ibarra on TEM analysis and Dr. Aldo Craievich on SAXS data analysis is deeply acknowledged.

References

Bae KH, Park M, Do MJ, Lee N, Ryu JH, Kim GW, Kim C, Park TG, Hyeon T (2012) Chitosan oligosaccharide-stabilized ferrimagnetic iron oxide nanocubes for magnetically modulated cancer hyperthermia. ACS Nano 6(6):5266–5273. doi:10.1021/nn301046w

Barbeta VB, Jardim RF, Kiyohara PK, Effenberger FB, Rossi LM (2010) Magnetic properties of Fe_3O_4 nanoparticles coated with oleic and dodecanoic acids. J Appl Phys 107(7):073913. doi:10.1063/1.3311611

Benkoski JJ, Bowles SE, Korth BD, Jones RL, Douglas JF, Karim A, Pyun J (2007) Field induced formation of mesoscopic polymer chains from functional ferromagnetic colloids. J Am Chem Soc 129(19):6291–6297. doi:10.1021/ja070779d

Bonini M, Fratini E, Baglioni P (2007) SAXS study of chain-like structures formed by magnetic nanoparticles. Mater Sci Eng, C 27(5–8):1377–1381. doi:10.1016/j.msec.2006.09.002

Borchert H, Shevchenko EV, Robert A, Mekis I, Kornowski A, Grübel G, Weller H (2005) Determination of nanocrystal sizes: a comparison of TEM, SAXS, and XRD studies of highly monodisperse $CoPt_3$ particles. Langmuir 21(5):1931–1936. doi:10.1021/la0477183

Chen SH, Teixeira J (1986) Structure and fractal dimension of protein-detergent complexes. Phys Rev Lett 57: 2583–2586. doi:10.1103/PhysRevLett.57.2583

Coey JMD (1971) Noncollinear spin arrangement in ultrafine ferrimagnetic crystallites. Phys Rev Lett 27:1140–1142. doi:10.1103/PhysRevLett.27.1140

Croucher MD, Hair ML (1977) Hamaker constants and the principle of corresponding states. J Phys Chem 81(17): 1631–1636. doi:10.1021/j100532a006

Evans W, Prasher R, Fish J, Meakin P, Phelan P, Keblinski P (2008) Effect of aggregation and interfacial thermal resistance on thermal conductivity of nanocomposites and colloidal nanofluids. Int J Heat Mass Transfer 51(5–6): 1431–1438. doi:10.1016/j.ijheatmasstransfer.2007.10.017

Faure B, Salazar-Alvarez G, Bergstrom L (2011) Hamaker constants of iron oxide nanoparticles. Langmuir 27(14): 8659–8664. doi:10.1021/la201387d

Freltoft T, Kjems JK, Sinha SK (1986) Power-law correlations and finite-size effects in silica particle aggregates studied by small-angle neutron scattering. Phys Rev B 33:269–275. doi:10.1103/PhysRevB.33.269

Gilbert B, Lu G, Kim CS (2007) Stable cluster formation in aqueous suspensions of iron oxyhydroxide nanoparticles. J Colloid Interface Sci 313(1):152–159. doi:10.1016/j.jcis.2007.04.038

Gonzalez-Fernandez MA, Torres TE, Andrs-Vergs M, Costo R, de la Presa P, Serna CJ, Morales MP, Marquina C, Ibarra MR, Goya GF (2009) Magnetic nanoparticles for power absorption: Optimizing size, shape and magnetic properties. J Solid State Chem 182(10):2779–2784. doi:10.1016/j.jssc.2009.07.047

Haase C, Nowak U (2012) Role of dipole-dipole interactions for hyperthermia heating of magnetic nanoparticle ensembles. Phys Rev B 85:045–435. doi:10.1103/PhysRevB.85.045435

Hamaker HC (1937) The Londonvan der Waals attraction between spherical particles. Physica 4(10):1058–1072. doi:10.1016/S0031-8914(37)80203-7

Huang TC, Toraya H, Blanton TN, Wu Y (1993) X-ray powder diffraction analysis of silver behenate, a possible low-angle diffraction standard. J Appl Crystallogr 26(2):180–184. doi:10.1107/S0021889892009762

Kellermann G, Vicentin F, Tamura E, Rocha M, Tolentino H, Barbosa A, Craievich A, Torriani I (1997) The small-angle X-ray scattering beamline of the Brazilian Synchrotron Light Laboratory. J Appl Crystallogr 30(5-2):880–883. doi:10.1107/S0021889897001829

Kim BH, Lee N, Kim H, An K, Park YI, Choi Y, Shin K, Lee Y, Kwon SG, Na HB, Park JG, Ahn TY, Kim YW, Moon WK, Choi SH, Hyeon T (2011) Large-scale synthesis of uniform and extremely small-sized iron oxide nanoparticles for high-resolution t1 magnetic resonance imaging contrast agents. J Am Chem Soc 133(32):12624–12631. doi:10.1021/ja203340

Kruglyakov PM (2000) Chapter 2 Stabilising ability of surfactants in emulsification and foam formation. In: Kruglyakov PM (ed) Hydrophile-Lipophile balance of surfactants and solid particles physicochemical aspects and applications, studies in interface science, vol 9, Elsevier, pp 100–145, doi:10.1016/S1383-7303(00)80015-0

Kruse T, Krauthäuser HG, Spanoudaki A, Pelster R (2003a) Agglomeration and chain formation in ferrofluids: two-dimensional X-ray scattering. Phys Rev B 67:094,206. doi:10.1103/PhysRevB.67.094206

Kruse T, Spanoudaki A, Pelster R (2003b) Monte carlo simulations of polydisperse ferrofluids: cluster formation and field-dependent microstructure. Phys Rev B 68:054208. doi:10.1103/PhysRevB.68.054208

Kwak K, Kim C (2005) Viscosity and thermal conductivity of copper oxide nanofluid dispersed in ethylene glycol. Rheology 17(2):35–40

Orthaber D, Bergmann A, Glatter O (2000) SAXS experiments on absolute scale with Kratky systems using water as a secondary standard. J Appl Crystallogr 33(2):218–225. doi:10.1107/S0021889899015216

Park J, An K, Hwang Y, Park JG, Noh HJ, Kim JY, Park JH, Hwang NM, Hyeon T (2004) Ultra-large-scale syntheses of monodisperse nanocrystals. Nat Mater 3(12):891–895

Pshenichnikov AF, Mekhonoshin V (2001) Cluster structure and the first-order phase transition in dipolar systems monte carlo simulation. Eur Phys J E 6:399–407. doi:10.1007/s10189-001-8053-5

Roca AG, Morales MP, O'Grady K, Serna CJ (2006) Structural and magnetic properties of uniform magnetite nanoparticles prepared by high temperature decomposition of organic precursors. Nanotechnology 17(11):2783. doi:10.1088/0957-4484/17/11/010

Rosensweig RE (1997) Ferrohydrodynamics. Dover books on physics. Dover Publications, New York. http://books.google.com.ar/books?id=uSa5nJGXYicC

Rosensweig RE (2002) Heating magnetic fluid with alternating magnetic field. J Magn Magn Mater 252(0):370–374. doi:10.1016/S0304-8853(02)00706-0

Shen L, Stachowiak A, Fateen SEK, Laibinis PE, Hatton TA (2001) Structure of alkanoic acid stabilized magnetic fluids. A small-angle neutron and light scattering analysis. Langmuir 17(2):288–299. doi:10.1021/la9916732

Sun S, Zeng H, Robinson DB, Raoux S, Rice PM, Wang SX, Li G (2004) Monodisperse MFe_2O_4 (M = Fe, Co, Mn) nanoparticles. J Am Chem Soc 126(1):273–279. doi:10.1021/ja0380852

Torres TE, Roca AG, Morales MP, Ibarra A, Marquina C, Ibarra MR, Goya GF (2010) Magnetic properties and energy absorption of $CoFe_2O_4$ nanoparticles for magnetic hyperthermia. J Phys Conf Ser 200(7):072,101. doi:10.1088/1742-6596/200/7/072101

Verde EL, Landi GT, Gomes JA, Sousa MH, Bakuzis AF (2012) Magnetic hyperthermia investigation of cobalt ferrite nanoparticles: Comparison between experiment, linear response theory, and dynamic hysteresis simulations. J Appl Phys 111(12):123902–123910. doi:10.1063/1.4729271

Weinstein JS, Varallyay CG, Dosa E, Gahramanov S, Hamilton B, Rooney WD, Muldoon LL, Neuwelt EA (2010)

Superparamagnetic iron oxide nanoparticles: diagnostic magnetic resonance imaging and potential therapeutic applications in neurooncology and central nervous system inflammatory pathologies, a review. J Cereb Blood Flow Metab 30(1):15–35. doi:10.1038/jcbfm.2009.192

Wu N, Fu L, Su M, Aslam M, Wong KC, Dravid VP (2004) Interaction of fatty acid monolayers with cobalt nanoparticles. Nano Lett 4(2):383–386. doi:10.1021/nl035139x

Zubarev AY, Odenbach S, Fleischer J (2002) Rheological properties of dense ferrofluids. Effect of chain-like aggregates. J Magn Magn Mater 252(0):241–243. doi:10.1016/S0304-8853(02)00674-1